



HAL
open science

The antibiotic cyclomarin blocks arginine-phosphate-induced millisecond dynamics in the N-terminal domain of ClpC1 from *Mycobacterium tuberculosis*

Katharina Weinhäupl, Martha Brennich, Uli Kazmaier, Joël Lelièvre, Lluís Ballell, Alfred Goldberg, Paul Schanda, Hugo Fraga

► To cite this version:

Katharina Weinhäupl, Martha Brennich, Uli Kazmaier, Joël Lelièvre, Lluís Ballell, et al.. The antibiotic cyclomarin blocks arginine-phosphate-induced millisecond dynamics in the N-terminal domain of ClpC1 from *Mycobacterium tuberculosis*. *Journal of Biological Chemistry*, 2018, 10.1074/jbc.RA118.002251 . hal-01768184

HAL Id: hal-01768184

<https://hal.science/hal-01768184>

Submitted on 17 Apr 2018

HAL is a multi-disciplinary open access archive for the deposit and dissemination of scientific research documents, whether they are published or not. The documents may come from teaching and research institutions in France or abroad, or from public or private research centers.

L'archive ouverte pluridisciplinaire **HAL**, est destinée au dépôt et à la diffusion de documents scientifiques de niveau recherche, publiés ou non, émanant des établissements d'enseignement et de recherche français ou étrangers, des laboratoires publics ou privés.

The antibiotic cyclomarin blocks arginine-phosphate–induced millisecond dynamics in the N-terminal domain of ClpC1 from *Mycobacterium tuberculosis*

Katharina Weinhäupl¹, Martha Brennich², Uli Kazmaier³, Joel Lelievre⁴, Lluís Ballell⁴, Alfred Goldberg⁵
Paul Schanda^{1*} and Hugo Fraga^{1,5,6*}

1-Institut de Biologie Structurale, Univ. Grenoble Alpes, CEA, CNRS, IBS, 71 Avenue des martyrs, F-38044 Grenoble, France

2-European Molecular Biology Laboratory, Grenoble, France

3- Institute of Organic Chemistry, Saarland University, Campus C4.2, 66123 Saarbrücken, Germany

4- Diseases of the Developing World, Glaxo Smith and Kline, Severo Ochoa 2, 28760 Tres Cantos, Madrid, Spain

5- Department Cell Biology, Harvard Medical School, USA

6- Departamento de Bioquímica, Faculdade de Medicina da Universidade do Porto, Portugal

Running Title: Cyclomarin blocks Arginine-Phosphate induced dynamics

Keywords: nuclear magnetic resonance, *Mycobacterium tuberculosis*, natural product, antibiotic action, antibiotic resistance, small angle X-ray scattering, protease, chaperone

* to whom correspondence should be addressed: hfraga@med.up.pt (H.F); paul.schanda@ibs.fr (P.S.)

Abstract:

Mycobacterium tuberculosis can remain dormant in the host, an ability that explains the failure of many current tuberculosis treatments. Recently, the natural products cyclomarin, ecumicin, and lassomycin have been shown to efficiently kill *Mycobacterium tuberculosis* persisters. Their target is the N-terminal domain of the hexameric AAA+ ATPase ClpC1, which recognizes, unfolds, and translocates protein substrates, such as proteins containing phosphorylated arginine residues, to the ClpP1P2 protease for degradation. Surprisingly, these antibiotics do not inhibit ClpC1 ATPase activity, and how they cause cell death is still unclear. Here, using NMR and

small-angle X-ray scattering, we demonstrate that arginine-phosphate binding to the ClpC1 N-terminal domain induces millisecond dynamics. We show that these dynamics are caused by conformational changes and do not result from unfolding or oligomerization of this domain. Cyclomarin binding to this domain specifically blocks these N-terminal dynamics. On the basis of these results, we propose a mechanism of action involving cyclomarin-induced restriction of ClpC1 dynamics, which modulates the chaperone enzymatic activity leading eventually to cell death.

Introduction:

Tuberculosis (TB) is a major public health problem with ten million people infected and two million dying each year (1). The main challenge in TB treatment is the long duration of therapy required for a cure, as the resistance of TB results from its ability to stay dormant for long periods in the host. Most antibiotics require bacterial replication for their action and this dormant state renders *Mycobacterium tuberculosis* (*Mtb*) resistant to bactericidal antibiotics. Aggravating this problem, *Mtb* has become increasingly resistant to existing antibiotics, and multidrug-resistant TB (MDR-TB) is now widespread (1).

The proteolytic complex formed by the proteins *Mtb*ClpP1 and *Mtb*ClpP2 and their hexameric regulatory ATPases, *Mtb*ClpX and *Mtb*ClpC1 are essential in mycobacteria and have emerged as attractive targets for anti-TB drug development. The Clp ATP-dependent protease complex is formed by two heptameric rings of protease subunits (*Mtb*ClpP1 and *Mtb*ClpP2) enclosing a central degradation chamber, and a hexameric ATPase complex, *Mtb*ClpC1 or *Mtb*ClpX (2). The ClpC1/ClpX ATPases recognize, unfold and translocate specific protein substrates into the *Mtb*ClpP1P2 proteolytic chamber, where degradation occurs. *Mtb*ClpC1 is a member of the class II AAA+ family of proteins, which contains a N-terminal domain (NTD) and two distinct ATP-binding modules, D1 and D2 (Fig. 1a). The active form of ClpC is a homohexamer, and in *Mtb*ClpC1 and *Synechococcus elongates* ClpC ATP alone is essential and sufficient for efficient protein degradation in association with ClpP (3). However, *B. subtilis* ClpC (*Bs*ClpC) requires the binding of both ATP and the adaptor protein MecA for formation of the active hexamer. No homologous adaptor protein has been described in *Mtb* (4) but it remains to be tested if *Mtb*ClpC1 can associate with a MecA-like protein.

Recently, Clausen and coworkers demonstrated that *Bs*ClpC specifically recognizes proteins phosphorylated on arginine residues by the arginine kinase McsB (5). These phosphorylation sites are often found in secondary structure elements and thus are accessible only when the

protein is unfolded or misfolded. This innovative work revealed a new pathway for selective degradation of misfolded proteins in bacteria, but the structural consequences of arginine-phosphate (ArgP) binding to ClpC are unclear. Indeed, although the crystal structure of *Bs*ClpC NTD shows two ArgP molecules bound to the protein, no significant structural changes were observed, which is quite surprising since arginine-phosphorylated substrates (e.g. casein) can stimulate *Bs*ClpC ATPase activity and can promote complex oligomerization (5).

The potential importance of *Mtb*ClpC1 as a novel drug target against TB has been emphasized by the recent findings by two independent groups that pyrazinamide (PZA) resistant strains contain mutations (Fig. 1b) in ClpC1 (6, 7). PZA is a critical first-line TB drug used with isoniazid, ethambutol and rifampicin for the treatment of TB and is also frequently used to treat MDR-TB (1). In addition to PZA, three natural product antibiotics that specifically target *Mtb*ClpC1 have been recently discovered: cyclomarin (8, 9), ecumicin (10) and lassomycin (11). Cyclomarin, identified (and since synthesized by independent groups) is bactericidal against TB and is able to kill non-replicating bacteria (9). Despite the absence of resistance mutations, ClpC1 NTD was identified as the drug target using affinity chromatography with cyclomarin conjugated to sepharose (9). While the crystal structure of the NTD was identical with or without cyclomarin bound, observations in *Mycobacterium smegmatis* suggested that cyclomarin can increase proteolysis by the ClpC1P1P2 machine (8, 9). How cyclomarin binding to the NTD may lead to increased proteolysis is still not known. Ecumicin is another potent natural antibiotic that efficiently kills *Mtb* persisters, and resistance mutations in ClpC fall within its NTD (fig 1b). When tested *in vitro*, ecumicin increases ClpC1 ATPase activity several fold, while simultaneously compromising degradation of ClpC1P1P2 substrates (10, 12). Lassomycin, an actinomycetes ribosomally encoded cyclic peptide, is yet another natural antibiotic able to kill *Mtb* persisters with efficiency (11). Despite

differing structurally from ecumicin, lassomycin also activates ATP hydrolysis by ClpC1 ATPase and resistant mutants map to a basic domain in the protein's NTD (11).

Due to their high molecular weights and structural complexity, these natural products are challenging for structure-activity relationship studies, but compounds with similar modes of actions may be very attractive as drug candidates. Comprehension of the mechanism of action of these compounds will provide valuable insights for development of more effective TB drugs. Unfortunately, the intrinsic flexibility and exchange dynamics between different oligomeric states of ClpC1 impeded so far structural studies. For example, crystallization of *BsClpC* was only possible upon the removal of flexible loop regions, rendering the protein nonfunctional, and at the same time underlining the importance of dynamics for the function of these complexes (13). For this purpose, nuclear magnetic resonance (NMR) and small angle X-ray scattering (SAXS) offer important advantages to investigate protein conformation in solution and test the effects of ligands.

Here we study the interaction of these potent new antibiotics with ClpC1 by using state of the art NMR and SAXS in order to elucidate their mode of action. A proper comprehension of the ways these drugs influence ClpC1 mechanism may also clarify how the family of AAA+ ATPases functions upon substrate binding.

Results:

Drug Binding to ClpC1 NTD

It is now widely accepted that conformational heterogeneity of proteins can be an important factor in ligand binding and drug mechanism of action (14). Indeed, in the case of cyclomarin, no significant changes of the ClpC1 NTD X-ray structure were observed upon ligand binding. Therefore, it was proposed that hidden unexplored conformations could be the basis for

the compound's specific actions (8). Although linking conformational heterogeneity or dynamics to protein function is a difficult task, NMR is a powerful method to elucidate such phenomena.

Full length *MtbClpC1* contains 849 residues that form a functional hexamer of 561 kDa in the presence of ATP. The large size of this complex together with its low solubility and expression prohibit NMR studies of the full-length protein, even when perdeuterated and specifically methyl labelled samples are used. To circumvent this problem, we cloned and expressed separately the *MtbClpC1* domains: NTD (1-145 aa), D1 (165-493 aa), D2 (494-849 aa), NTD-D1 (1-493 aa) and D1-D2 (165-849 aa). With the exception of the NTD, NTD-D1 and D2 constructs, all the other yielded insoluble proteins when expressed. Moreover, the D2 domain when purified did not show any detectable ATPase activity and did not form oligomers in the presence of ATP, while the NTD-D1 construct was soluble when expressed in ArticExpress cells at 4 °C, but precipitated when ATP was added.

Mutations in the NTD of *MtbClpC1* have been shown to confer resistance to cyclomarin, ecumicin, lassomycin and PZA, indicating a pivotal role of this domain (Fig1b). This 16 kDa domain is easily accessible for solution state NMR even without perdeuteration. Therefore, we focused our work on *MtbClpC1* NTD and tested the effects of the different antibiotics on its structure in solution. *MtbClpC1* NTD behaved as a homogeneous monomeric protein upon size exclusion chromatography (FigS1a) and dynamic light scattering (DLS, FigS1a), and resulted in high quality NMR spectra with excellent peak dispersion, indication of a well-folded, globular protein (Fig2a). Two sets of assignment experiments were done. While at pH 7.5, we were unable to assign loop regions due to amide exchange, at pH 6.0 we were able to assign 95% of all residues allowing the mapping of almost the entire protein structure. ClpC1 NTD consists of eight helices that fold as two repeats of a four-helix motif sharing 58% identity (Fig2b). A 14 amino acid loop between helix 4 and 5 connects

the two motifs (8). Analysis of the backbone ^1H , ^{13}C and ^{15}N chemical shifts with TALOS+ (15) shows that the predicted secondary structure elements in the NTD in solution are highly similar to the elements in the crystal structure (Fig2b).

We proceeded testing the effect of cyclomarin binding on *MtbClpC1* NTD spectra. When cyclomarin was added to the *MtbClpC1* NTD, large changes in the spectrum were observed (Fig2a). Similar changes were observed with the analogue desoxycyclomarin (Fig S1b)(16). In fact, given the amplitude of chemical shift perturbations (CSP), a new set of assignment experiments was required to identify the shifted residues. The large magnitude of the CSP (Fig2c) observed is likely a consequence of the rich content of aromatic residues in the cyclomarin molecule and the corresponding ring-current effect. As the chemical shift is very sensitive to a change in the local chemical environment, we were able to map the compound binding site to the region between helix 1 and 5 (Fig2d) in agreement with the X-ray structure of this domain in the presence of bound cyclomarin (8). Analysis of the backbone amide, CO, $\text{C}\alpha$ and $\text{C}\beta$ chemical shifts with TALOS+ (15) shows that the predicted secondary structure elements in the cyclomarin bound NTD in solution are highly similar to the elements in the crystal structure (Fig S1d) excluding major changes in the domain secondary structure.

Based on the location of the resistance mutations (Fig1b), ecumicin was proposed to target the *MtbClpC1* NTD as well (10). For this reason, we tested if we could observe similar effects for ecumicin, as we did for cyclomarin by NMR. Compared to cyclomarin, ecumicin only caused modest spectral changes (Fig S2). These small perturbations did not indicate a strong binding of ecumicin to the *MtbClpC1* NTD and were inconsistent with previous biochemical data where ecumicin was found to be a potent inhibitor of *MtbClpC1* degradation of casein, but a stimulator of *MtbClpC1* ATPase activity (result confirmed here, Fig S2d) (10). Consequently, we tested ecumicin binding to the NTD using

isothermal titration calorimetry (ITC). While we were able to confirm the nanomolar K_d for cyclomarin (8) (Fig S3), we were unable to obtain a saturation curve with ecumicin under the conditions used (up to 100 μM ecumicin, Fig S3). In contrast to cyclomarin and ecumicin, the addition of PZA did not result in any changes of NTD NMR spectra, furthermore no binding of PZA was observed by ITC (Fig S3).

NTD dynamics

Analysis of ^{15}N backbone relaxation rates can provide detailed information about protein dynamics on different time scales. In particular motions in the μs -ms timescale, associated with conformational changes between different states, often occur in sites important for protein function (17, 18). Studying the dynamics of *MtbClpC1* NTD is particularly interesting, since it acts as a ligand recognition site that has to convey information about the bound state to the D1 and D2 rings for ATP driven translocation and unfolding. Given the very modest structural differences of the NTD in its apo and cyclomarin bound states, we reasoned that dynamics may be important in the allosteric process.

In order to investigate whether such μs -ms motions are indeed relevant for the NTD, we performed Carr-Purcell-Meiboom-Gill (CPMG) relaxation-dispersion (RD) NMR experiments. Briefly, RD profiles monitor the effective spin relaxation rate constant ($R_{2,eff}$) as a function of a variable repetition rate, ν_{CPMG} , of refocusing pulses applied during a relaxation delay. The presence of conformational dynamics is manifest as a dependence of $R_{2,eff}$ on ν_{CPMG} , i.e. “non-flat” RD profiles. Such dispersions arise when the local environment around the atom under consideration is fluctuating on a μs -ms time scale, either because of motion of the considered atom(s) or neighboring atoms, e.g. through binding events. When we applied this technique to apo NTD, we observed flat RD curves for all backbone amides. Thus, this domain alone does not exhibit significant μs -ms motions.

Furthermore, cyclomarin binding does not induce ms dynamics in the NTD.

Arginine-Phosphate and arginine phosphorylated proteins bind to *MtbClpC1* NTD

In *B.subtilis* phosphorylation of arginines targets certain proteins for ClpCP-mediated degradation (5). Phosphorylated proteins, are first detected and bound by the NTD of ClpC and then transferred to the D1 domain for subsequent unfolding and degradation (5). Analyzing the *MtbClpC1* NTD sequence, we found that the binding site of ArgP in *B. subtilis* is strictly conserved in *Mtb* (Fig3a). Furthermore, comparing the overall structures of the two NTDs, it is clear that they are structurally identical with an RMSD of 1.7 Å (Fig S3b). This striking similarity motivated us to test if *MtbClpC1* NTD could also bind ArgP. Indeed, using ITC we confirmed that NTD could bind ArgP with a K_d of 5.2 μM (Fig3b), a similar value as reported for *BsClpC* NTD (5). In addition, a pull down showed that McsB phosphorylated lysozyme and casein bind to ClpC1 NTD while no binding was observed with the control substrate (Fig 3c). Furthermore, as previously reported for *BsClpC*, a large excess of free ArgP was required to inhibit this association likely reflecting a stronger binding of NTD to the protein substrate (Fig 3c). Despite some residual binding of non-phosphorylated lysozyme, a similar result was observed when full length ClpC1 was used instead of isolated NTD (Fig S3c).

Addition of ArgP to *MtbClpC1* NTD resulted in strong perturbations of its backbone amide NMR spectrum (Fig 3d). This effect was specific to ArgP since no significant changes were observed with unmodified arginine or phosphoserine (Fig S4). In contrast to the rather small changes in peak intensity observed upon cyclomarin or ecumicin addition, ArgP caused large changes in peak intensity, with 45% of the peaks falling below the level of detection into the background noise (Fig 3e). As shown below, this decrease in intensity can indicate exchange events at the affected residues. Interestingly, these residues do not map exclusively to the putative binding site of ArgP,

but are localised over a large part of the core of the structure, whereby helices 2, 3, 6 and 7 are most affected (Fig3e, 3f). Using CPMG RD experiments, we could prove that the observed decrease in intensity is indeed caused by millisecond dynamics (Fig 4a, 4b). Surprisingly, these dynamics can be seen throughout the domain. In Fig. 4a the affected residues and the $\Delta R_{2\text{eff}}$ are plotted on the structure of *MtbClpC1* NTD. Furthermore, we assume that the part of the protein showing the highest degree of motion are the three helices with disappearing resonances (refer to Fig3f).

Although CPMG RD experiments provide residue resolved direct evidence of the motions, they do not actually reveal what the underlying motion corresponds to. In the case of low affinity binding, ms dynamics can be also caused by on/off binding dynamics of the compound. Considering the ArgP K_d , we can calculate the population of free NTD with the concentrations of ArgP used (2 mM), which results in full domain saturation (calculated free NTD 0.3 %). Fitting of the CPMG RD data with the software Chemex provides an exchange rate between the ground and excited state, the population of the excited state and the chemical shift difference between the two states. The fitted population of the excited state (5 %, Fig S5d) is not in agreement with the calculated free state of the NTD (0.3 %). Moreover, theoretical chemical shift differences of the excited state derived from fitting of the CPMG RD data with Chemex do not correlate with experimental chemical shift differences between apo and ArgP bound NTD (Fig S5a). To conclude, we confirmed that the excited state does not correspond to the free state of the NTD, but most likely to a different conformation.

Arginine has been previously reported to reduce the melting point of some protein but paradoxically has been also suggested as a stabilizer for protein preparations (19-22). In order to discard the possibility that the dynamics observed result from ArgP promoted unfolding we recorded far-UV circular dichroism (CD) spectra of *MtbClpC1* NTD with and without ArgP present. In both cases, the spectra were typical for α -helical proteins with characteristic minima

at ≈ 210 nm and ≈ 222 nm (Fig. 5a). Additionally, we used chemical shift differences from the Chemex fitting of the CPMG RD data and compared these values with the chemical shift differences of the folded NTD and calculated random coil shifts derived from nclDP (23) (FigS5b). Clearly, the fitted chemical shift differences do not correlate with the calculated random coil values. Thus, ArgP does not appear to unfold the NTD and also does not perturb the secondary structure of the domain. Alternatively, ArgP might induce domain oligomerization, which would explain peaks disappearing by transient interactions between two ClpC1 subunits. Analysis of the protein by DLS (FigS1) and Diffusion Ordered Spectroscopy (DOSY, FigS5e), however, excluded this hypothesis. Both ArgP and cyclomarin did not induce any change in *MtbClpC1* NTD oligomerization.

Intrinsic aromatic fluorescence can be used to probe conformational changes upon ligand binding. While *MtbClpC1* NTD does not contain any tryptophan residues, it contains 3 tyrosine residues (Y27, Y102 and Y145), which can be used as probes for domain conformational changes (Fig S5f). When we tested the effect of ArgP on NTD fluorescence, we observed an increase in tyrosine fluorescence (Fig S5g) associated with a stabilization of the protein. NTD displayed cooperative unfolding with an apparent T_m of 69 °C, this value was increased to 79 °C in the presence of ArgP 1 mM (Fig 5b).

An alternative approach to probe conformational changes is the use of fluorescent probes. 1-Anilidonaphthalene-8-Sulfonic Acid (ANS) binds to hydrophobic regions in the protein, and ANS fluorescence increases substantially when proteins undergo changes that expose hydrophobic surfaces as normally occurs during protein unfolding. ANS can, however, be used to detect subtle conformational changes, and we tested if ArgP binding leads to changes in ANS fluorescence. While ANS binding to *MtbClpC1* NTD resulted in an increase in fluorescence, indicating the presence of exposed hydrophobic surface, ArgP binding did not significantly alter fluorescence (Fig5c). Because cyclomarin has

intense intrinsic fluorescence, it cannot be used in the previous fluorescence studies.

Cyclomarin restricts ArgP-induced dynamics

The fact that cyclomarin binding does not affect *MtbClpC1* NTD dynamics is inconsistent with the prior proposal that cyclomarin acts by causing conformational changes in this domain (8). By contrast, ArgP leads to a significant increase in domain dynamics. We therefore tested if cyclomarin binding could either block ArgP-recognition or ArgP-induced dynamics. Adding ArgP to *MtbClpC1* NTD prebound to cyclomarin, we observed significant changes in the ^1H - ^{15}N correlated HSQC spectrum in the binding site of ArgP (Fig S6). This is consistent with our pull-down results where no effect of cyclomarin on arginine phosphorylated proteins binding to the NTD was observed (Fig3c). However, the behavior of ArgP bound and ArgP/cyclomarin bound NTD was clearly different. Several peaks that disappeared upon ArgP binding, reappeared when cyclomarin was added. Instead of 45%, only 25% of all peaks disappeared when cyclomarin was added together with ArgP. Related to the spectral changes, the most striking difference between ArgP and ArgP/cyclomarin binding are the dynamic properties of the NTD. When ArgP is bound to the NTD most observed residues exhibit μs -ms dynamics. These dynamics can however be completely abolished by addition of cyclomarin. In ArgP/cyclomarin bound NTD, not a single residue showed μs -ms dynamics exactly as occurs in apo *MtbClpC1* NTD (Fig 4). Cyclomarin binds to a hydrophobic “bed” formed by two phenylalanines in the symmetric axis of the domain (8), which by stabilizing the core of the domain, presumably explains how it can block completely NTD domain dynamics.

Cyclomarin prevents ArgP inhibition of FITC-casein degradation

The primary function of ClpC1 is to recognize certain cellular proteins and to unfold and translocate them into ClpP1P2 for degradation, although it is also able, at least *in vitro*, to catalyze the refolding of some proteins (2, 24). Until the discovery of ArgP in *BsClpC* no recognition signal for ClpC was known. In the presence of the cofactor MecA, *BsClpC* can catalyze the degradation of unfolded proteins, such as casein. However, ArgP (1mM) is able to block MecA-dependent proteolysis, apparently because the binding site of ArgP overlaps with the contact site of MecA and *BsClpC*'s NTD (5). This observation clearly suggests that ClpC has two alternative mechanisms for substrate selection. One for unfolded proteins containing no specific tag and dependent on the MecA adaptor for efficient ClpC1 oligomerization and activation, and a second MecA-independent pathway that depends specifically on the presence of protein sequences containing phosphorylated arginines (5, 25). In contrast to *BsClpC*, *MtbClpC1* does not require any cofactor for activity. In the presence of ATP it can, in association with *MtbClpP1P2*, efficiently degrade unfolded proteins like casein (2).

Despite these differences, the mechanism of these homologous enzymes seems to be conserved between species, and studying the effects of cyclomarin and ArgP on protein degradation by *MtbClpC1P1P2* could give important mechanistic insights.

One interesting question that arises is whether ArgP binding is able to block casein degradation as it does in *BsClpC*. We therefore compared degradation of FITC-casein in the presence and absence of ArgP. ArgP caused a significant inhibition (up to 55%, Fig5d) of FITC-casein degradation, but it did not completely block this process even at very high ArgP concentrations. By contrast, in the presence of cyclomarin (20 μ M), no inhibition of proteolysis was observed (Fig5d).

ClpC1 forms high oligomeric species in solution

We used SAXS as a complementary method to obtain information on the effect of drug binding on ClpC1 structure. Compared to X-ray

diffraction, SAXS has a modest resolution but can provide information on several global parameters: the radius of gyration; the largest intraparticle distance; the particle shape; and the degree of folding, denaturation, or disorder (26). All these parameters can be good reporters for significant structural changes promoted by drug binding. In addition, SAXS does not require the preparation of highly concentrated deuterated samples, allowing the study of ClpC1 structure in native like solution conditions.

Our first SAXS measurements in batch format in the presence of ATP revealed the presence of very high molecular weight species incompatible with a ClpC1 hexamer. As *MtbClpC1* is inherently prone to aggregation, known to seriously affect SAXS data interpretation, we concluded that part of the *MtbClpC1* sample could be aggregated. To overcome this problem, we turned to size-exclusion chromatography coupled to SAXS (SEC-SAXS). In this system, the sample is separated according to size and shape before SAXS measurement, this way removing protein aggregates from the protein samples. Indeed, consistent with the aggregation hypothesis, when ClpC1 was loaded on a Superose 6 10/300 GL column, the chromatograms of ClpC1 showed two distinct peaks: a small peak directly after the void volume followed by a second broad peak (Fig 6a). The scattering signal at the second peak was relatively stable with a radius of gyration in the range of 8 nm (Table S1), but reduces significantly to 7.6 nm at the end of the peak, indicating either structural flexibility or overlapping oligomeric states. Surprisingly, this radius of gyration was again clearly inconsistent with a ClpC1 hexamer (radius of gyration 5.53 nm) representing instead bigger complexes. Apparently, in the conditions used (Hepes 50 mM pH 7.5, KCl 100 mM, glycerol 10%, MgCl₂ 4 mM and ATP 1 mM, ClpC 1 mg/ml), the hexamer is not the dominant species, and ClpC1 appears to exist in a rather distinct molecular organization. Recently, Carroni et al, using cryo-electron microscopy (cryo-EM) and mutagenesis, showed that *S. aureus* ClpC (*SaClpC*) can exist in a decameric resting state formed through ClpC middle domains establishing intermolecular

head-to-head contacts (27). This head to head contacts allow the docking of two layers of ClpC molecules arranged in a helical conformation. Despite their oligomerization, these structures are however highly dynamic - as the peripheral subunits are likely in exchange – suggesting that higher order species can exist in equilibrium.

As the middle domain of *MtbClpC1* is conserved compared to *SaClpC*, and to better understand how our SAXS data could relate to the resting state cryo-EM structure, we averaged frames from the center of the peak and the trailing end. SAXS estimates the molecular weight at the center of the peak between 1100 and 1400 kDa, compatible with 12- or 14-mers (Table S1). For the tail, the estimated weight between 860 and 1200 kDa is in better agreement with 10- or 12-mers. Bead modeling based on both curves resulted in curling stone shaped objects, whose main body matches the reported EM data in size and shape (Fig6b). An artifact resulting from the presence of several oligomer populations in the sample is observed in the form of an appendix. Direct comparison of the SAXS curve from the tail with the atomistic model gives a surprisingly good fit ($\chi^2=3.4$, Fig 6c), given that the SAXS curve represents an ensemble of states. Considering the similarities between our data and the previously reported cryo-EM structure, it is likely that *MtbClpC1* can form a resting state with a large part of the population representing even higher oligomers than decamers. This difference could derive from a concentration dependent oligomeric equilibrium which would explain why *MtbClpC1* seems larger in our study as compared to the SEC-MALS data presented by Carroni et al (27). In fact, crosslinking data from the same study already suggested the presence of complexes bigger than the EM decameric structure (27). While we could not detect the hexamer in solution, the fact that in the same conditions ClpC1 is active, catalyzing the degradation of GFP_{ssra} and casein in association with ClpP1P2, suggests that a part of the population exists as a hexamer.

We proceeded testing if the natural product antibiotics or ArgP targeting ClpC1 could affect

the distribution of ClpC1 between a resting state and an active hexameric form. The addition of ecumicin (20 μ M), cyclomarin (20 μ M) and ArgP (200 μ M) to the SEC buffer lead only to small changes in the averaged SAXS curve (Fig S8 & Table S1). As the curve is not stable, the differences are too small to allow any statement about local structural rearrangement. It appears however that the natural antibiotics tested do not affect the ClpC1 oligomer equilibrium significantly.

Discussion:

The structural characterization of AAA+ proteins involved in molecular recognition and unfolding is usually a complex task. Whereas their intrinsic heterogeneity normally results in difficult crystallization, their oligomeric organization and large size makes their study by NMR challenging. So far, no X-ray structure is available for *MtbClpC1* and, as reported here, the full-length protein and its domains have intrinsic low solubility. Adding further complexity to the study of the system, we show here that *MtbClpC1* can exist in an equilibrium between different oligomeric states. The existence of a resting decameric state formed by the association of head-to-head contacts between coiled-coil middle domains of ClpC was recently described by Carroni et al (27). The middle domains were proposed to repress the activity of ClpC by forming a highly dynamic resting state that can block substrate binding or ClpP interaction. Quite striking is the observation that a single point mutation in the middle domain can disrupt the resting state and result in the formation of an active hexamer even in the absence of the MecA adaptor (27). Consistent with the conservation of the key residues between *MtbClpC1* and *SaClpC* (27), our SAXS data suggests that a similar structure is predominant versus the active hexameric form in *MtbClpC1*. However, contrary to the case of *S. aureus* or *B. subtilis*, where MecA was proposed to modulate this equilibrium, in the case of *Mtb* it is not clear how the distribution between resting state and hexameric

form occurs. N-terminal domains are packed between middle domains in this resting state, and were suggested to play a role in the complex stability by fluctuating between a hidden position to an exposed one, available to adaptors or substrates. One hypothesis is that the equilibrium could be modulated by substrates or natural product antibiotics. However, we could show that the addition of cyclomarin, ecumicin or ArgP ligand appears not to shift ClpC1 distribution. With the current data, we cannot exclude that binding of a bulkier substrate can shift the equilibrium towards a state where the NTDs are not constrained thus activating the unfoldase.

Whereas natural product antibiotics appear not to influence ClpC1 oligomerization equilibrium, we were unable to obtain convincing evidence for ecumicin or PZA binding to the isolated *MtbClpC1* NTD. This result is intriguing, as mutations in the NTD domain have been associated with resistance to ecumicin and PZA (10). With regard to ecumicin, we and others (10) were able to demonstrate biochemical activity, namely activating ATPase activity. Most likely, ecumicin requires full length ClpC1 or an oligomeric structure for binding and ATPase activation. Possibly the binding site is located at the interface of the NTD and D1 domain, which can explain the ATPase activation by ecumicin. In this case, disrupting part of the binding site, the N-terminal interface in the resistant mutants, might be sufficient for reduced binding affinity *in vivo*. Small CSPs were evident on the NTD NMR spectrum for ecumicin in the regions where resistant mutations are located, suggesting that this region could be part of the putative binding site (FigS2). In the case of PZA, an efficient “dirty drug” with multiple reported cellular targets, we cannot exclude that resistance derives from the modulation of protein homeostasis for any of the other targets, for example preventing or increasing substrate degradation (28).

Using NMR, we could show that, although cyclomarin binds with high affinity to the ClpC1 NTD, the domain dynamics are not modified. *MtbClpC1* NTD is a rather rigid domain, and

showed no millisecond dynamics in the apo state. Also, cyclomarin binding does not result in peak broadening or loss of intensity that might indicate the presence of an alternative state. These observations rule out the existence of hidden conformations not captured by previous X-ray studies (8).

Finally, our finding that ArgP binding induces millisecond dynamics in the *MtbClpC1* NTD domain is a new and important clue about ClpC1 mechanisms. Particularly when no alternative conformations were reported in the X-ray structure of *BsClpC* with ArgP-bound, and because no structural changes were observed with arginine or phosphoserine. While we excluded unfolding and transient-binding as potential explanations for the observed dynamics, we were unable to pursue structural determination since approximately half of the residues in the ArgP-bound NTD are NMR invisible. ArgP binding results in a significant increase in tyrosine fluorescence and a dramatic change in the stability of this domain. While the increased fluorescence could result from subtle changes in tyrosine side chains in a region densely packed with aromatic residues (three Phe and two Tyr, FigS5) the increased stability could derive from the ArgP binding preferentially to the folded state. The exact relationship between ArgP induced dynamics and the functional cycle of *MtbClpC1* is currently not clear. Do dynamics promote target binding through ArgP recognition by allowing multiple transient interaction sites with the incoming substrate? Conformational heterogeneity and dynamics in substrate binding sites have been proposed to increase substrate recognition efficiency, and at the same time to facilitate substrate handover to downstream elements, by making a multitude of transient weak interactions with the substrate which can be easily broken (29). In fact, a single phosphorylated arginine in a protein has been shown to be sufficient for efficient ClpC-mediated degradation. Thus ClpC’s molecular recognition mechanism must be highly efficient, for example 1 mM of free ArgP does not completely block protein binding, which may appear inconsistent

with the micromolar K_d that we and others report for ArgP binding to the isolated NTD (5). Despite this, the fact that cyclomarin cannot block arginine phosphorylated protein binding appears to contradict the hypothesis that dynamics are fundamental for substrate association to the NTD, not excluding however, that they are relevant for subsequent steps – for example substrate release to the D1 pore (Fig 7). Another possibility is that the observed conformational dynamics could modulate the positioning of the NTD related to the D1 pore. Indeed, studies with the type II eukaryotic homologue p97/Cdc48 ATPase complex which shares the NTD-D1-D2 architecture with ClpC1, have stressed the mechanistic relevance of the interface between NTD/D1 and the denominated up/down equilibrium of the highly mobile NTDs (30). In p97/Cdc48, NTDs have been shown to adopt, depending on the nucleotide bound, either a coplanar (down) or elevated (up) position with respect to the D1 domain (30). Increasing the life time of the NTDs “up state”, thereby holding the substrate next to the D1 pore would promote substrate recognition, while supporting the down state would prevent substrate recognition, nevertheless exposing the D1 domain pore. In *E.coli* ClpA, a close bacterial homologue of ClpC, removal of NTD is known to seriously impair recognition of substrates bearing the SsrA-targeting sequence, but to have only a modest

Experimental Procedures:

ArgP was obtained from Sigma. Cyclomarin and desoxycyclomarin were synthesized as previously described (33). *MtbClpC1*, *MtbClpP1*, *MtbClpP2* were expressed and purified as previously described (2). *Bacillus stearothermophilus* mcsB was cloned into a pet28a+ vector and expressed and purified as previously described (5). *MtbClpC1* domains: NTD corresponding to residues 1-145, D1 corresponding to residues 165-493, D2 corresponding to residues 494-849, NTD-D1 corresponding to 1-493 and D1-D2 corresponding to 165-849 were cloned into a pet28a+ vector by Genscript. Unless otherwise noted, the purification protocol consisted of an

effect on degradation of unfolded proteins (31). In other words, NTDs may work as recognition domains for certain substrates, while at the same time blocking the D1 domain and preventing free access for unfolded proteins. This differential effect on certain substrates was the basis for the suggested role for the NTDs as an “entropic brush” that prevents nonspecific degradation of proteins by blocking access to the D1 ring (32). In our view the competition between recognition of ArgP-labelled and unfolded protein, can simultaneously explain the inhibition of casein degradation by ArgP, and the effect of cyclomarin, which is able to completely abolish this inhibition of casein hydrolysis.

Put together, our work shows that ArgP binding to *MtbClpC1*NTD leads to widespread domain millisecond dynamics and that cyclomarin is able to block this process. While, it is surely not the absence of ClpC1 NTD dynamics that kills TB but likely its derived functional consequences, for example blocking the ArgP pathway, this work sheds light on ClpC mechanism. Rather than a static interaction, ArgP labelled proteins binding to ClpC must be understood as a highly dynamic process. Cyclomarin is therefore a unique example of a drug whose mode of action relies on the restriction of protein dynamics induced by substrate binding.

initial NiNTA affinity chromatography step taking advantage of the histidine tag, followed by a size exclusion step using a Hiloal 16/600 Superdex 200 pg column. FITC-casein, GFPssra degradation and ATP hydrolysis were measured, as previously described (2). For DLS measurements, 200 μ l of a 1.1 mg/ml ClpC1 NTD solutions with and without ArgP (1 mM) were used.

Far UV CD spectra were acquired on a Jasco J-810 spectropolarimeter continuously purged with nitrogen and thermostated at 20 °C. Briefly, a solution of ClpC1 NTD (5 μ M) in Tris pH 7.5 NaCl 150 mM with/without ArgP (1 mM) was used to obtain CD spectra between 205 and 250 nm.

Intrinsic tyrosine fluorescence was measured in a Varian Cary Eclipse spectrofluorimeter using a 60

μM solution of ClpC1 NTD. Samples were excited at 280 nm, and fluorescence spectra were measured from 290 to 350 nm. Samples in the presence of ANS (50 μM) were excited at 370 nm, and fluorescence spectra were measured from 400 to 600 nm.

Degree of saturation of ClpC1 NTD

The degree of saturation of ClpC1 NTD with ArgP was calculated using the equation:

$$\frac{[PL]}{[P]} = \frac{1}{2} \left[1 + \frac{[L]_0}{[P]_0} + \frac{K_d}{[P]_0} - \sqrt{\left(1 + \frac{[L]_0}{[P]_0} + \frac{K_d}{[P]_0} \right)^2 - 4 \frac{[L]_0}{[P]_0}} \right]$$

where $[L]_0$ is initial ligand, $[P]_0$ is initial protein and PL is protein ligand complex.

SAXS data collection and analysis

SEC-SAXS data were collected at ESRF BM29 (34, 35). The HPLC system (Shimadzu, France) was directly coupled to the 1.8 mm flow-through capillary of SAXS exposure unit. The flow rate for all online experiments was 0.3 mL/min. SAXS data collection was performed continuously throughout the chromatography run at a frame rate of 1 Hz with a Pilatus 1M detector (Dectris) at the distance of 2.876 m from the capillary. The scattering of pure water was used to calibrate the intensity to absolute units (36). The X-ray energy was 12.5 keV and the accessible q -range 0.07 nm^{-1} to 4.9 nm^{-1} . The incoming flux at the sample position was in the order of 10^{12} photons/s in $700 \times 700 \mu\text{m}^2$. A summary of the acquisition parameters is given in table S1. All images were automatically azimuthally averaged with pyFAI (37) and corrected for background scattering by the online processing pipeline (38). For each frame, the forward scattering intensity and radius of gyration were determined according to the

Guinier approximation (https://github.com/kif/freesas). For each run, regions of 20 to 80 frames were averaged for further characterization. Data at small angles before the Guinier-region was removed before further data analysis to avoid experimental artefacts.

Pair distribution functions were calculated using GNOM (39). 20 ab-initio models each were calculated in C1 symmetry, using DAMMIF (40) and averaged, aligned and compared using DAMAVER (41). The scattering curve of the ClpC decamer (27) was predicted and fitted to experimental data using Crysol 3 (42).

NMR experiments

All NMR experiments were performed on Bruker Avance III spectrometers, equipped with cryogenically cooled TCI probeheads, operating at magnetic field strengths corresponding to ^1H Larmor frequencies of 850, 700 and 600 respectively. The sample temperature was set to 37 °C, unless stated otherwise.

Sequence-specific resonance assignments of ClpC1 NTD

Apo ClpC1 NTD was assigned in NMR buffer pH 6 (50mM MES, 100mM NaCl, 5% D_2O) and in NMR buffer pH 7.5 (50mM Tris, 50mM NaCl, 5% D_2O) at a protein concentration of 0.8mM at a ^1H Larmor frequency of 600. The following experiments were performed: 2D ^{15}N - ^1H BEST HSQC, 3D BEST HNCO, 3D BEST-TROSY HNcaCO, 3D BEST HNCA, 3D BEST HNcoCA, 3D BEST HNcoCACB and 3D BEST HNCACB (43).

The same experimental conditions were used for the assignment of ClpC1 NTD in the presence of cyclomarin, except for a lower protein concentration due to low solubility of cyclomarin (0.2 mM ClpC1 NTD, 0.22 mM cyclomarin). DMSO controls were also measured.

For the assignment of ClpC1 NTD in the presence of ArgP and ArgP plus cyclomarin, ^{15}N - ^1H BEST HSQC, BEST HNCO and BEST HNCA spectra were

recorded at a ^1H Larmor frequency of 850 MHz. Assignment was performed by following the chemical shifts of backbone amide, C_α and CO peaks in apo and ligand bound spectra. The sample conditions used were: 0.2 mM ClpC1 NTD and 2 mM ArgP or 0.2 mM ClpC1 NTD, 2 mM ArgP and 0.22 mM cyclomarin in NMR buffer pH 6.

Data processing and analysis were performed using the NMRPipe software package (44) and CCPN software (45).

Titration of cyclomarin into *MtbClpC1* NTD:

For the cyclomarin titration four titration points were measured with 0.2 mM *MtbClpC1* NTD each. The DMSO content in all samples was 2.2 %. The measured ratios between the NTD and cyclomarin were 1:0, 1:1.1, 1:1.5 and 1:2. No chemical shift changes were observed after a ratio of 1:1.1 *MtbClpC1* NTD:cyclomarin. Ratio used for experiments 1:1.1.

Titration of ArgP into *MtbClpC1* NTD:

Five titration points were measured with 0.3 mM *MtbClpC1* NTD each. The DMSO content in all samples was 0.6 %. The measured ratios between the NTD and ArgP were 1:0, 1:0.5, 1:1, 1:2 and 1:10. No intensity changes were observed after a ratio 1:2 *MtbClpC1* NTD : ArgP. Ratio used for experiments 1:10.

Titration of cyclomarin and ArgP into *MtbClpC1* NTD:

Four different samples were measured for the titration of *MtbClpC1* NTD with cyclomarin and ArgP. All samples contained 4.2 % DMSO and 0.2 mM *MtbClpC1* NTD. We measured one reference sample, one sample with 0.22 mM cyclomarin added, one sample with 0.22 mM cyclomarin and 0.2 mM ArgP and one sample containing 0.22 mM cyclomarin and 2 mM ArgP.

Titration of Ecumicin into *MtbClpC1* NTD:

Three titration points were measured with 0.2 mM *MtbClpC1* NTD each. The DMSO content in all samples was 4 %. The measured ratios between the NTD and Ecumicin were 1:0, 1:1, and 1:2. Due to the insolubility of Ecumicin no higher concentrations of Ecumicin could be measured.

Titration of Pyrazinamide into *MtbClpC1* NTD:

Three titration points were measured with 0.2 mM *MtbClpC1* NTD each. The DMSO content in all samples was 2 %. The measured ratios between the NTD and ArgP were 1:0, 1:1 and 1:10. No intensity or chemical shift changes were observed at any measured Pyrazinamide concentration.

BEST-TROSY type (43) ^{15}N CPMG relaxation dispersion experiments were performed with the pulse scheme described by Franco et al (46) at static magnetic field strengths of 700 and 850 MHz, at a sample temperature of 37 °C. Effective relaxation rate constants, $R_{2\text{eff}}$, were measured at 11 (700 MHz) and 13 (850 MHz) different CPMG frequencies and derived from the commonly employed two-point measurement scheme (47), $R_{2\text{eff}} = -1/T \cdot \ln(I/I_0)$, where I is the peak intensities in the experiment with the CPMG pulse train and I_0 the one in a reference experiment without relaxation delay. T is the total relaxation delay, which was chosen as 60 ms and 40 ms in the experiments performed at 700 and 850 MHz, respectively. Peak heights and error margins were extracted in the software nmrView (OneMoon Scientific). A two-state exchange model was fitted jointly to the dispersion data of 24 residues using the program ChemEx (48). Briefly, the program involves the integration of the Bloch-McConnell equations throughout the explicit train of CPMG pulses, taking into account offset effects and finite pulse lengths. Error estimates were obtained from Monte Carlo simulations. The fit curves from the joint fit are shown in Fig S7, and a table of residue-wise chemical-shift differences is provided in Fig S5c.

Acknowledgments:

Hugo Fraga is a COFUND fellowship recipient co-funded by the European Union and the Tres Cantos Open Lab Foundation (TC189). This work used the platforms of the Grenoble Instruct center (ISBG; UMS 3518 CNRS-CEA-UJF-EMBL) with support from FRISBI (ANR-10-INSB-05-02) and GRAL (ANR-10-LABX-49-01) within the Grenoble Partnership for Structural Biology (PSB). Special thanks to Dr Caroline Mas for valuable advises. Dr. Goldberg's lab has received grants from the Tres Cantos Open Lab Foundation and National Institute of General Medical Sciences. We thank the ESRF for beamtime at BM29.

Author contributions:

KW, MB and HF conceived and performed experiments, KW, MB, UK, JL, LB, AG, LB, PS and HF analyzed the data, KW and HF wrote the manuscript.

Declaration of Interests:

The authors declare no competing interests.

References:

1. Zumla, A., Nahid, P., and Cole, S. T. (2013) Advances in the development of new tuberculosis drugs and treatment regimens. *Nat Rev Drug Discov.* **12**, 388–404
2. Akopian, T., Kandror, O., Raju, R. M., Unnikrishnan, M., Rubin, E. J., and Goldberg, A. L. (2012) The active ClpP protease from *M. tuberculosis* is a complex composed of a heptameric ClpP1 and a ClpP2 ring. *The EMBO Journal.* **31**, 1529–1541
3. Andersson, F. I., Blakytyn, R., Kirstein, J., Turgay, K., Bukau, B., Mogk, A., and Clarke, A. K. (2006) Cyanobacterial ClpC/HSP100 protein displays intrinsic chaperone activity. *J Biol Chem.* **281**, 5468–5475
4. Kirstein, J., Schlothauer, T., Dougan, D. A., Lilie, H., Tischendorf, G., Mogk, A., Bukau, B., and Turgay, K. (2006) Adaptor protein controlled oligomerization activates the AAA+ protein ClpC. *The EMBO Journal.* **25**, 1481–1491
5. Trentini, D. B., Suskiewicz, M. J., Heuck, A., Kurzbauer, R., Deszcz, L., Mechtler, K., and Clausen, T. (2016) Arginine phosphorylation marks proteins for degradation by a Clp protease. *Nature.* 10.1038/nature20122
6. Yee, M., Gopal, P., and Dick, T. (2017) Missense Mutations in the Unfoldase ClpC1 of the Caseinolytic Protease Complex Are Associated with Pyrazinamide Resistance in *Mycobacterium tuberculosis*. *Antimicrob. Agents Chemother.* **61**, AAC.02342–16–6
7. Zhang, S., Chen, J., Shi, W., Cui, P., Zhang, J., Cho, S., Zhang, W., and Zhang, Y. (2017) Mutation in clpC1 encoding an ATP-dependent ATPase involved in protein degradation is associated with pyrazinamide resistance in *Mycobacterium tuberculosis*. *Nature Publishing Group.* **6**, e8
8. Vasudevan, D., Rao, S. P. S., and Noble, C. G. (2013) Structural basis of mycobacterial inhibition by cyclomarin A. *J Biol Chem.* **288**, 30883–30891
9. Schmitt, E. K., Riwanto, M., Sambandamurthy, V., Roggo, S., Miault, C., Zwingelstein, C., Krastel, P., Noble, C., Beer, D., Rao, S. P. S., Au, M., Niyomrattanakit, P., Lim, V., Zheng, J., Jeffery, D., Pethe, K., and Camacho, L. R. (2011) The Natural Product Cyclomarin Kills *Mycobacterium*

- Tuberculosis by Targeting the ClpC1 Subunit of the Caseinolytic Protease. *Angew. Chem. Int. Ed.* **50**, 5889–5891
10. Gao, W., Kim, J.-Y., Anderson, J. R., Akopian, T., Hong, S., Jin, Y.-Y., Kandror, O., Kim, J.-W., Lee, I.-A., Lee, S.-Y., McAlpine, J. B., Mulugeta, S., Sunoqrot, S., Wang, Y., Yang, S.-H., Yoon, T.-M., Goldberg, A. L., Pauli, G. F., Suh, J.-W., Franzblau, S. G., and Cho, S. (2015) The cyclic peptide ecumicin targeting ClpC1 is active against *Mycobacterium tuberculosis* in vivo. *Antimicrob. Agents Chemother.* **59**, 880–889
 11. Gavriš, E., Sit, C. S., Cao, S., Kandror, O., Spoering, A., Peoples, A., Ling, L., Fetterman, A., Hughes, D., Bissell, A., Torrey, H., Akopian, T., Mueller, A., Epstein, S., Goldberg, A., Clardy, J., and Lewis, K. (2014) Lassomycin, a Ribosomally Synthesized Cyclic Peptide, Kills *Mycobacterium tuberculosis* by Targeting the ATP-Dependent Protease ClpC1P1P2. *Chem Biol.* **21**, 509–518
 12. Jung, I.-P., Ha, N.-R., Kim, A.-R., Kim, S.-H., and Yoon, M.-Y. (2017) Mutation analysis of the interactions between *Mycobacterium tuberculosis* caseinolytic protease C1 (ClpC1) and ecumicin. *Int. J. Biol. Macromol.* **101**, 348–357
 13. Wang, F., Mei, Z., Qi, Y., Yan, C., Hu, Q., Wang, J., and Shi, Y. (2011) Structure and mechanism of the hexameric MecA-ClpC molecular machine. *Nature.* **471**, 331–335
 14. Hart, K. M., Ho, C. M. W., Dutta, S., Gross, M. L., and Bowman, G. R. (2016) Modelling proteins' hidden conformations to predict antibiotic resistance. *Nat Commun.* **7**, 12965
 15. Shen, Y., Delaglio, F., Cornilescu, G., and Bax, A. (2009) TALOS+: a hybrid method for predicting protein backbone torsion angles from NMR chemical shifts. *J Biomol NMR.* **44**, 213–223
 16. Barbie, P., and Kazmaier, U. (2016) Total synthesis of desoxycyclomarin C and the cyclomarazines A and B. *Org. Biomol. Chem.* **14**, 6055–6064
 17. Kleckner, I. R., and Foster, M. P. (2011) An introduction to NMR-based approaches for measuring protein dynamics. *Biochim Biophys Acta.* **1814**, 942–968
 18. Eisenmesser, E. Z., Millet, O., Labeikovsky, W., Korzhnev, D. M., Wolf-Watz, M., Bosco, D. A., Skalicky, J. J., Kay, L. E., and Kern, D. (2005) Intrinsic dynamics of an enzyme underlies catalysis. *Nature.* **438**, 117–121
 19. Ishibashi, M., Tsumoto, K., Tokunaga, M., Ejima, D., Kita, Y., and Arakawa, T. (2005) Is arginine a protein-denaturant? *Protein Expr. Purif.* **42**, 1–6
 20. Golovanov, A. P., Hautbergue, G. M., Wilson, S. A., and Lian, L.-Y. (2004) A simple method for improving protein solubility and long-term stability. *J. Am. Chem. Soc.* **126**, 8933–8939
 21. Shukla, D., and Trout, B. L. (2010) Interaction of arginine with proteins and the mechanism by which it inhibits aggregation. *J. Phys. Chem. B.* **114**, 13426–13438
 22. Vagenende, V., Han, A. X., Mueller, M., and Trout, B. L. (2013) Protein-associated cation clusters in aqueous arginine solutions and their effects on protein stability and size. *ACS Chem. Biol.* **8**, 416–422
 23. Tamiola, K., Acar, B., and Mulder, F. A. A. (2010) Sequence-specific random coil chemical shifts of intrinsically disordered proteins. *J. Am. Chem. Soc.* **132**, 18000–18003
 24. Kar, N. P., Sikriwal, D., Rath, P., Choudhary, R. K., and Batra, J. K. (2008) *Mycobacterium tuberculosis* ClpC1. *FEBS J.* **275**, 6149–6158
 25. Kirstein, J., Dougan, D. A., Gerth, U., Hecker, M., and Turgay, K. (2007) The tyrosine kinase McsB is a regulated adaptor protein for ClpCP. *The EMBO Journal.* **26**, 2061–2070
 26. Svergun, D. I., and Koch, M. H. J. (2003) Small-angle scattering studies of biological macromolecules in solution. *Reports on Progress in Physics.* **66**, 1735–1782
 27. Carroni, M., Franke, K. B., Maurer, M., Jäger, J., Hantke, I., Glöge, F., Linder, D., Gremer, S., Turgay, K., Bukau, B., and Mogk, A. (2017) Regulatory coiled-coil domains promote head-to-head assemblies of AAA+ chaperones essential for tunable activity control. *elife.* **6**, 741–24
 28. Zhang, Y., Shi, W., Zhang, W., and Mitchison, D. (2014) Mechanisms of Pyrazinamide Action and

- Resistance. *Microbiol Spectr.* **2**, MGM2–0023–2013
29. He, L., Sharpe, T., Mazur, A., and Hiller, S. (2016) A molecular mechanism of chaperone-client recognition. *Sci Adv.* **2**, e1601625–e1601625
 30. Schuetz, A. K., and Kay, L. E. (2016) A Dynamic molecular basis for malfunction in disease mutants of p97/VCP. *elife.* **5**, 653
 31. Lo, J. H., Baker, T. A., and Sauer, R. T. (2001) Characterization of the N-terminal repeat domain of Escherichia coli ClpA-A class I Clp/HSP100 ATPase. *Protein Sci.* **10**, 551–559
 32. Ishikawa, T., Maurizi, M. R., and Steven, A. C. (2004) The N-terminal substrate-binding domain of ClpA unfoldase is highly mobile and extends axially from the distal surface of ClpAP protease. *Journal of Structural Biology.* **146**, 180–188
 33. Barbie, P., and Kazmaier, U. (2016) Total Synthesis of Cyclomarin A, a Marine Cycloheptapeptide with Anti-Tuberculosis and Anti-Malaria Activity. *Org. Lett.* **18**, 204–207
 34. Pernot, P., Round, A., Barrett, R., De Maria Antolinos, A., Gobbo, A., Gordon, E., Huet, J., Kieffer, J., Lentini, M., Mattenet, M., Morawe, C., Mueller-Dieckmann, C., Ohlsson, S., Schmid, W., Surr, J., Theveneau, P., Zerrad, L., and McSweeney, S. (2013) Upgraded ESRF BM29 beamline for SAXS on macromolecules in solution. *J Synchrotron Radiat.* **20**, 660–664
 35. Brennich, M. E., Round, A. R., and Hutin, S. (2017) Online Size-exclusion and Ion-exchange Chromatography on a SAXS Beamline. *J Vis Exp.* 10.3791/54861
 36. Orthaber, D., Bergmann, A., and Glatter, O. (2000) SAXS experiments on absolute scale with Kratky systems using water as a secondary standard. *J Appl Crystallogr.* **33**, 218–225
 37. Ashiotis, G., Deschildre, A., Nawaz, Z., Wright, J. P., Karkoulis, D., Picca, F. E., and Kieffer, J. (2015) The fast azimuthal integration Python library: pyFAI. *J Appl Crystallogr.* **48**, 510–519
 38. Brennich, M. E., Kieffer, J., Bonamis, G., De Maria Antolinos, A., Hutin, S., Pernot, P., and Round, A. (2016) Online data analysis at the ESRF bioSAXS beamline, BM29. *J Appl Crystallogr.* **49**, 203–212
 39. Svergun, D. I. (1992) Determination of the regularization parameter in indirect-transform methods using perceptual criteria. *J Appl Crystallogr.* **25**, 495–503
 40. Franke, D., and Svergun, D. I. (2009) DAMMIF, a program for rapid ab-initio shape determination in small-angle scattering. *J Appl Crystallogr.* **42**, 342–346
 41. Volkov, V. V., and Svergun, D. I. (2003) Uniqueness of ab initio shape determination in small-angle scattering. *J Appl Crystallogr.* **36**, 860–864
 42. Franke, D., Petoukhov, M. V., Konarev, P. V., Panjkovich, A., Tuukkanen, A., Mertens, H. D. T., Kikhney, A. G., Hajizadeh, N. R., Franklin, J. M., Jeffries, C. M., and Svergun, D. I. (2017) ATSAS 2.8: a comprehensive data analysis suite for small-angle scattering from macromolecular solutions. *J Appl Crystallogr.* **50**, 1212–1225
 43. Favier, A., and Brutscher, B. (2011) Recovering lost magnetization: polarization enhancement in biomolecular NMR. *J Biomol NMR.* **49**, 9–15
 44. Delaglio, F., Grzesiek, S., Vuister, G. W., Zhu, G., Pfeifer, J., and Bax, A. (1995) NMRPipe: A multidimensional spectral processing system based on UNIX pipes. *J Biomol NMR.* **6**, 277–293
 45. Vranken, W. F., Boucher, W., Stevens, T. J., Fogh, R. H., Pajon, A., Llinas, M., Ulrich, E. L., Markley, J. L., Ionides, J., and Laue, E. D. (2005) The CCPN data model for NMR spectroscopy: development of a software pipeline. *Proteins: Structure, Function, and Bioinformatics.* **59**, 687–696
 46. Franco, R., Gil-Caballero, S., Ayala, I., Favier, A., and Brutscher, B. (2017) Probing Conformational Exchange Dynamics in a Short-Lived Protein Folding Intermediate by Real-Time Relaxation-Dispersion NMR. *J. Am. Chem. Soc.* **139**, 1065–1068
 47. Mulder, F. A., Mittermaier, A., Hon, B., Dahlquist, F. W., and Kay, L. E. (2001) Studying excited states of proteins by NMR spectroscopy. *Nat Struct Biol.* **8**, 932–935
 48. Bouvignies, G., and Kay, L. E. (2012) Measurement of proton chemical shifts in invisible states of

Figure Legends:

Figure 1. Structural model of *MtbClpC1* showing drug-resistant mutations in the N-terminal domain.

(a) Side and top view of *MtbClpC1* structural model based on *BsClpC* in complex with MecA (pdb 3j3s). In gray NTD and linker region, in blue D1 domain and in green D2 domain. NTD and linker are predicted to be mobile. (b) *MtbClpC1* NTD (pdb 3wdb) is the assumed target of the natural product antibiotics ecumicin, cyclomarin and lassomycin. Mutations in pyrazinamide-resistant strains have also been mapped to this domain. Depicted as pink spheres are ecumicin-resistant mutations (L92S, L96P, L92F) (10), in yellow, lassomycin-resistant (Q17R, Q17H, R21S, P79T) (11) and in green pyrazinamide-resistant (G99D (7) and L88V, G99D, I108T, R114L mutations (6)). The crystal structure of cyclomarin-bound *MtbClpC1* NTD is shown in Figure 2d.c) Binding site of cyclomarin (yellow) and ArgP (red) on the *MtbClpC1* NTD.

Figure 2. NMR assignment and cyclomarin-binding site of *MtbClpC1* NTD.

(a) ^1H - ^{15}N correlated backbone amide spectrum of apo (black) and cyclomarin bound (blue) *MtbClpC1* NTD. 95% of amide resonances of the apo and 79% of the cyclomarin bound protein spectrum have been assigned. (b) TALOS+ predicted helix propensity derived from NMR assignments of apo *MtbClpC1* NTD. In dark blue predicted helix, in white predicted loop and as a gray background helical parts in the X-ray structure of *MtbClpC1* NTD (PDB: 3wdb). The secondary structure in solution and in the crystal, seem to be identical. (c) Combined chemical shift difference between apo and cyclomarin-bound *MtbClpC1* NTD ^1H - ^{15}N HSQC spectra. Chemical shift differences are mapped on the structure in Figure 2d. (d) Chemical shift differences from Figure 2c plotted on the structure of cyclomarin bound *MtbClpC1* NTD (PDB: 3wdb). Assigned backbone amides are shown as spheres, and unassigned residues as gray cartoon. Chemical shift differences are plotted in a spectrum from blue to white, whereby blue indicates a strong effect. Cyclomarin is shown as yellow sticks

Figure 3. The effect of ArgP binding on *MtbClpC1* NTD.

(a) Sequence alignment of *MtbClpC1* NTD and *BsClpC* NTD. Identical residues are highlighted in black and similar residues in grey. The binding site of ArgP in *BsClpC* NTD is circled in red. (b) Representative Isothermal Calorimetry Titration of ArgP binding to *MtbClpC1* NTD ($N = 1.99 \pm 0.02$; $K_d = 5.2 \pm 0.5 \mu\text{M}$; $\Delta H = -4066 \pm 59 \text{ cal/mol}$; $\Delta S = 10.3 \text{ cal/mol/deg}$). (c) NTD is able to pull down lysozyme phosphorylated by McsB kinase but not non-treated lysozyme (lane 1 and 4). Cyclomarin ($50 \mu\text{M}$) is unable to block substrate binding but a reduction is observed with ArgP (1 mM). (d) ^1H - ^{15}N correlated backbone amide spectrum of apo (black), ArgP (green), cyclomarin (blue) and ArgP/cyclomarin (red) bound *MtbClpC1* NTD. 95% of apo, 55% ArgP, 85% of cyclomarin and 75% of CymA/ArgP bound *MtbClpC1* NTD amide resonances are NMR visible. (e) Loss in peak intensity of resonances in ^1H - ^{15}N HSQC spectra upon ArgP binding with (red) or without (green) cyclomarin added. (f) Peak height ratio of ArgP bound *MtbClpC1* NTD (Figure 3d, left) plotted on its structure (PDB: 3wdb). Assigned residues are shown as spheres, unassigned residues as gray cartoon, residues that disappear upon ArgP binding as white cartoon. Peak height ratio is drawn as a spectrum from green to white. Whereby white indicates loss in intensity. Two arginine-phosphate molecules (red sticks) are placed at the putative ArgP binding site, identical to the X-ray structure of *BsClpC* NTD (PDB: 5hbn).

Figure 4. ArgP induces millisecond dynamics in *MtbClpC1* NTD.

(a) Residues that exhibit millisecond dynamics plotted on the *MtbClpC1* NTD structure (PDB: 3wdb). All assigned residues are shown as spheres. Residues that have a $\Delta R_{2,eff}$ of 5 are in yellow, of 15 orange and of 30 or more red. (b) Examples of CPMG curves for residues with a $\Delta R_{2,eff}$ of 5, 15 or 30. Apo *MtbClpC1* NTD has no millisecond dynamics (lower row), 63% of all NMR visible residues experience ms dynamics when ArgP is bound (upper row), if cyclomarin is added before ArgP no more ms dynamics can be observed, resulting in flat dispersion curves (middle row).

Figure 5. Effect of ArgP on *MtbClpC1* NTD secondary structure and *MtbClpC1* substrate degradation.

(a) CD spectrum of apo (black) and ArgP bound (green) *MtbClpC1* NTD. ArgP binding does not influence the secondary structure of *MtbClpC1* NTD. (b) ArgP bound (green) is more stable than Apo *MtbClpC1* NTD. Intrinsic tyrosine fluorescence was measured as a function of temperature. (c) ArgP (green) does not change exposure of hydrophobic regions in *MtbClpC1* NTD (black). Shown in gray the fluorescence of ANS in buffer. (d) ArgP inhibits FITC-casein degradation by *MtbClpC1P1P2* (black curve). Cyclomarin (20 μ M) is able to block this inhibition (blue curve).

Figure 6. ClpC1 forms high oligomeric species in solution.

(a) SEC-SAX chromatogram of *MtbClpC1*, showing the radius of gyration of the eluted species (pink) with the respective absorbance at 280 nm (black). The first peak immediately after the column void volume corresponds to protein aggregates. (b) DAMMIF models obtained from *MtbClpC1* scattering curve in the presence of different ligands ecumicin (pink), cyclomarin (blue) and ArgP (green). With the exception of the appendix, an artifact derived from sample heterogeneity, the obtained model fits well to the structure obtained previously by Cryo-EM (pdb 6em9). (c) The scattering curve of the resting state *SaClpC* decamer was predicted and fitted using Crysol 3 to the experimental curve obtained from the apo*MtbClpC1* tail of the peak .

Figure 7. *MtbClpC1* exists in equilibrium between a resting state and a functional hexamer.

MtbClpC1 can form a resting state in equilibrium with the active hexameric form. Phosphorylation of arginines marks proteins for degradation by the ClpCP machinery. Phosphorylated arginines bind to the NTD where they induce millisecond dynamics that could either facilitate contact between different NTDs or the transfer of the substrate to the D1 domain pore. Although, cyclomarin binding does not change the structure of the NTD or substrate binding it restricts ArgP induced dynamics.

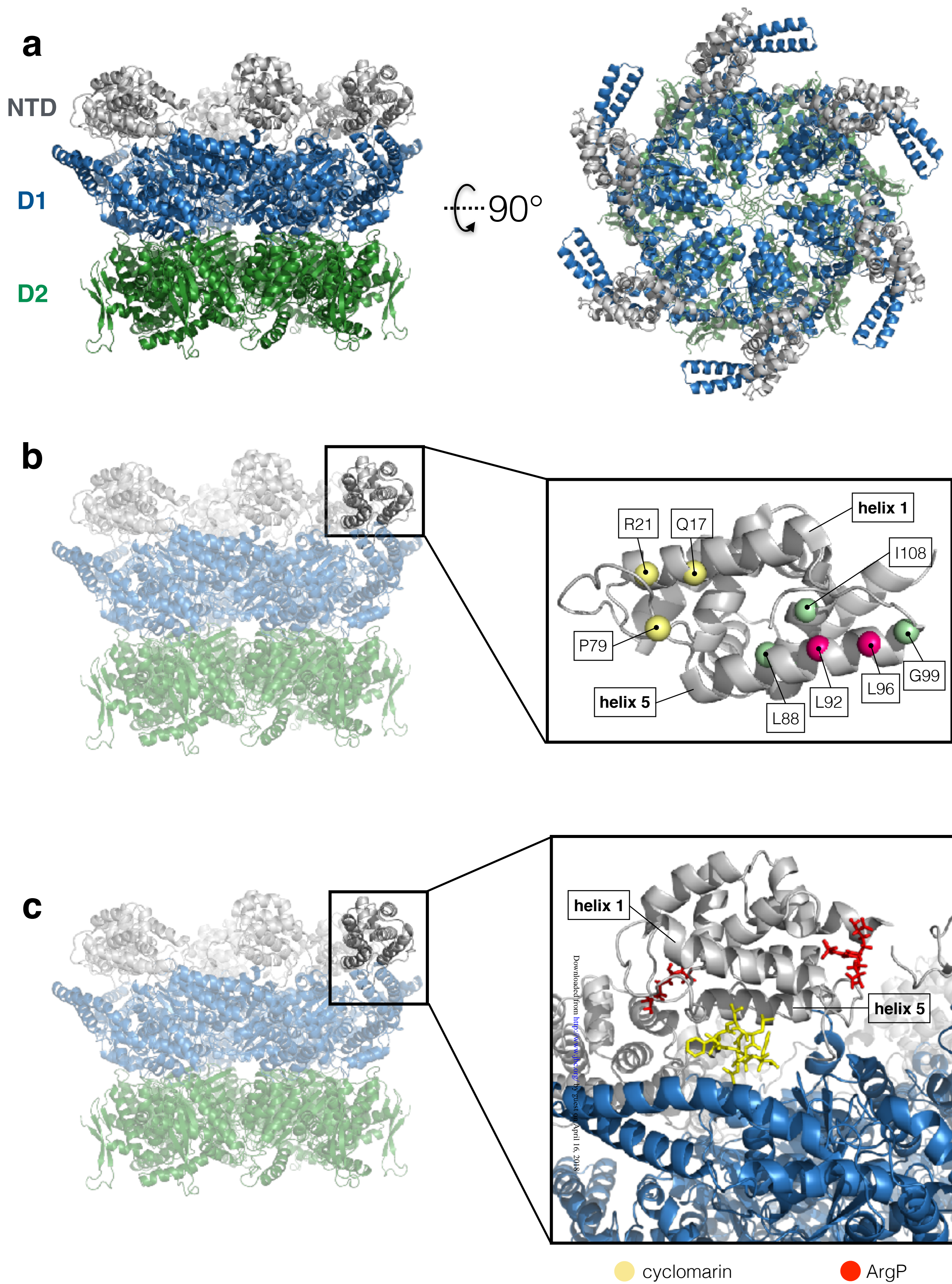
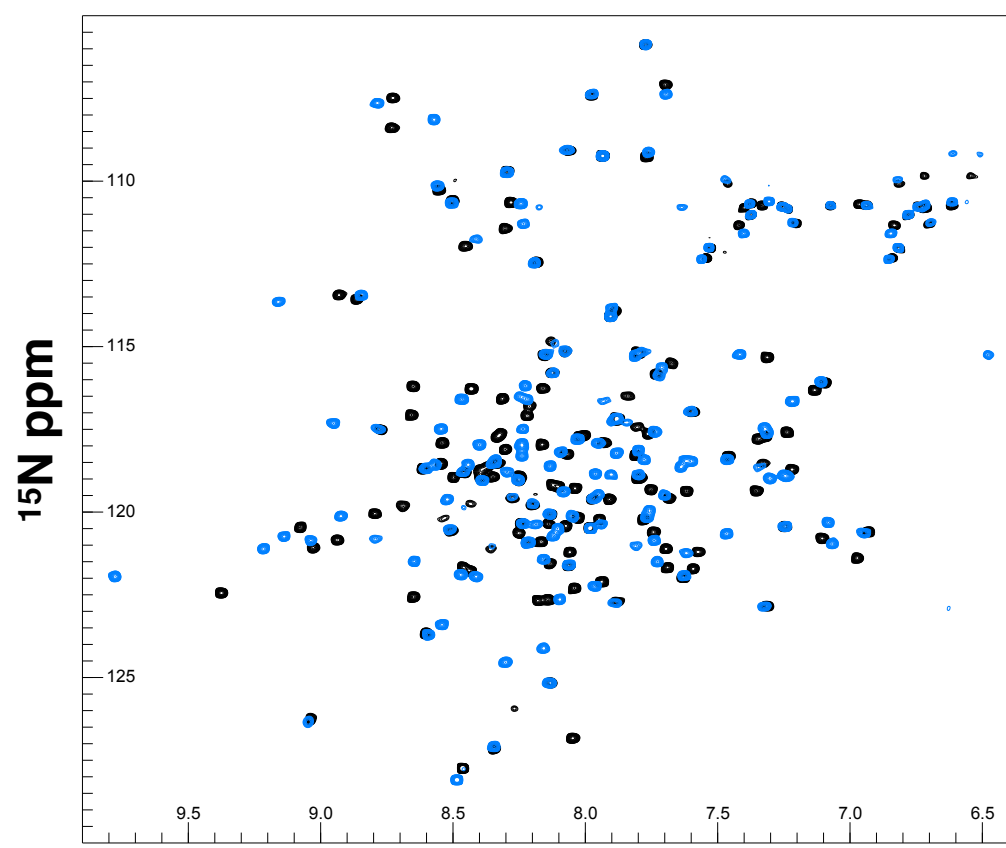
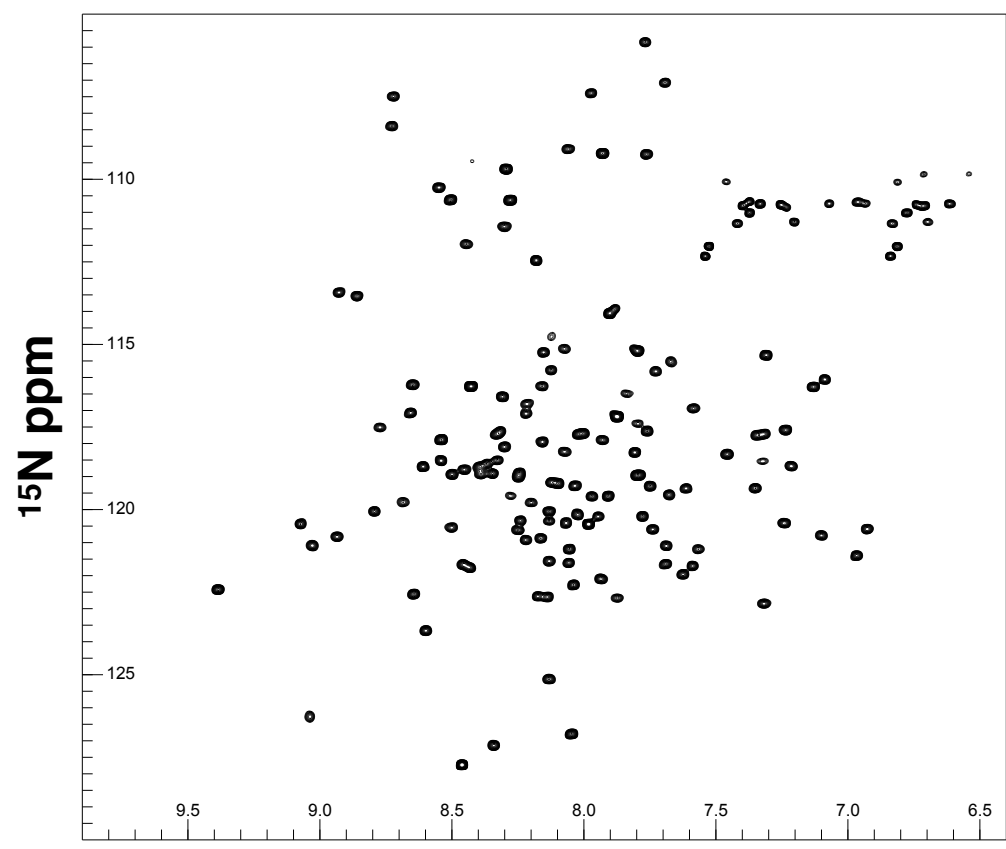


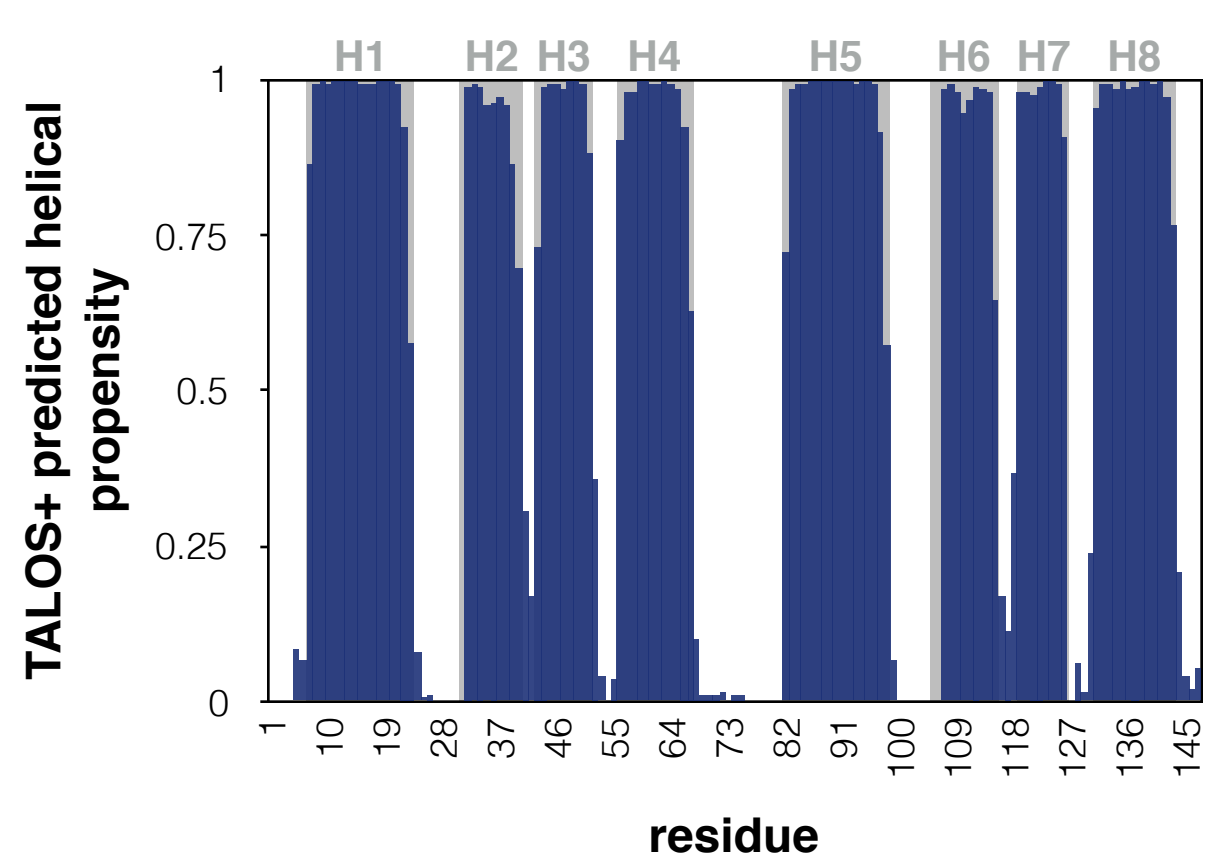
Figure 1

a ● apo ClpC1 NTD ● +cyclomarin

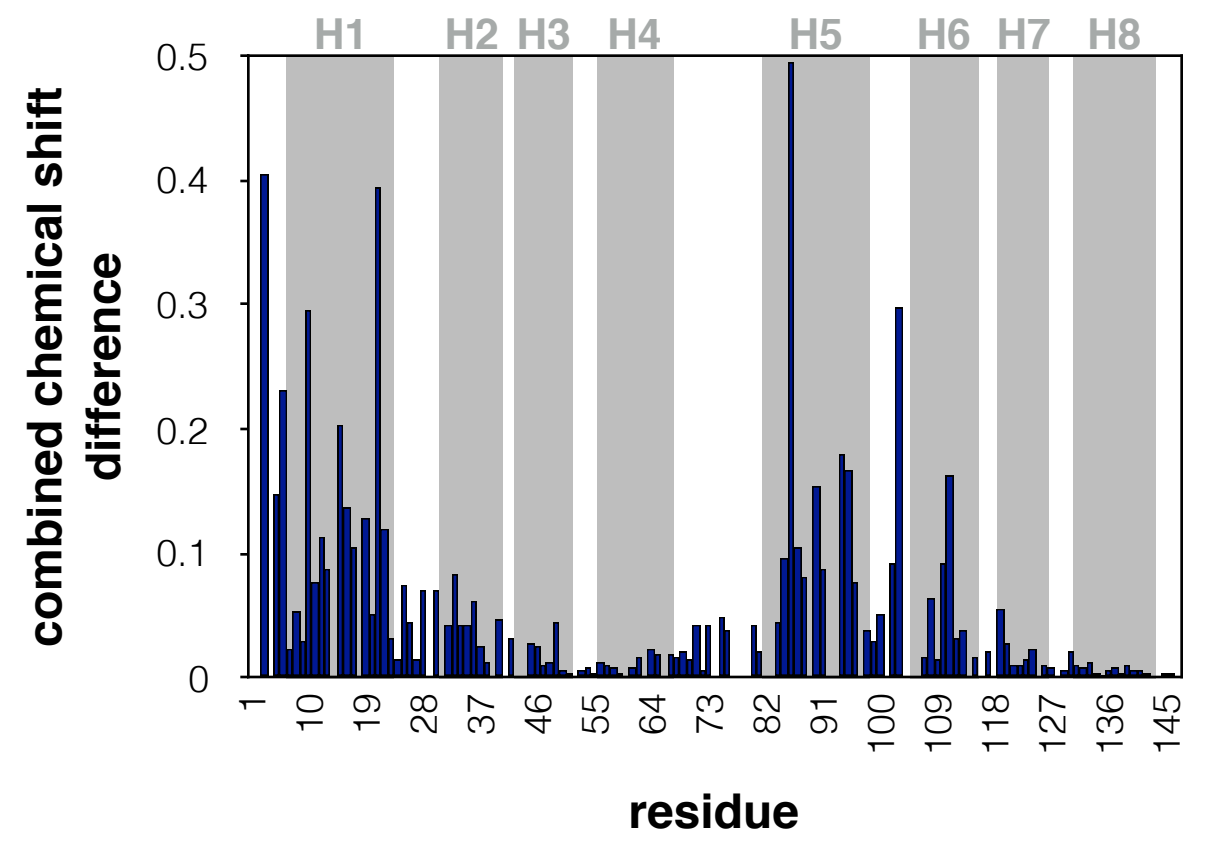


^1H ppm

b ● helix ○ loop ● helix in X-ray structure



c



d

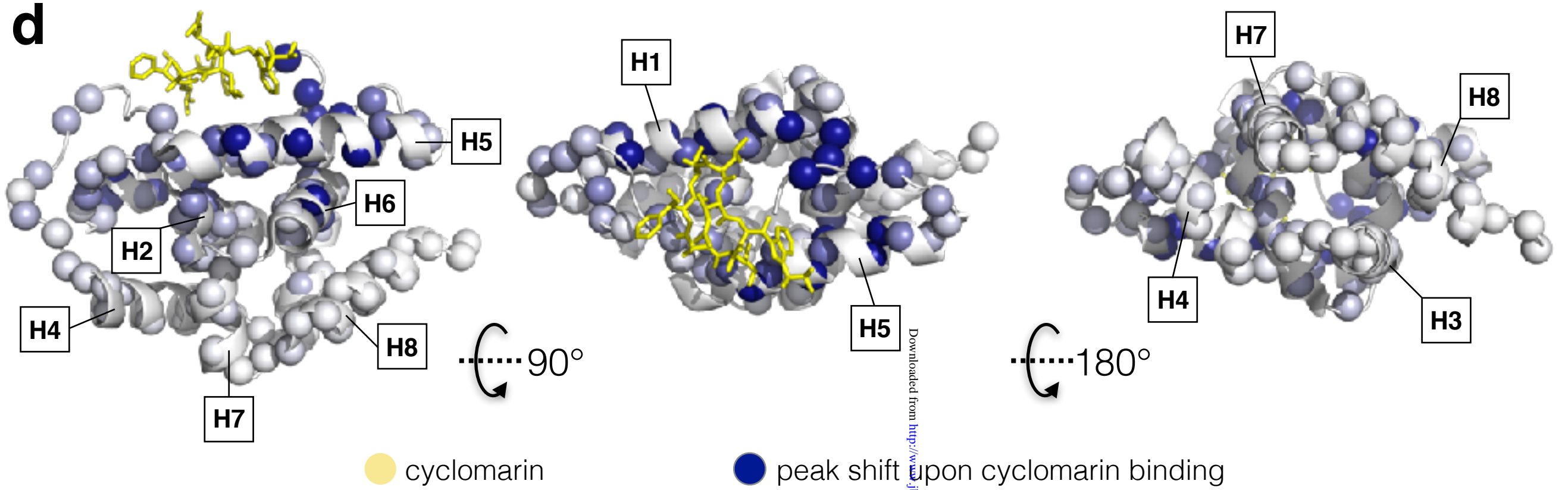


Figure 2

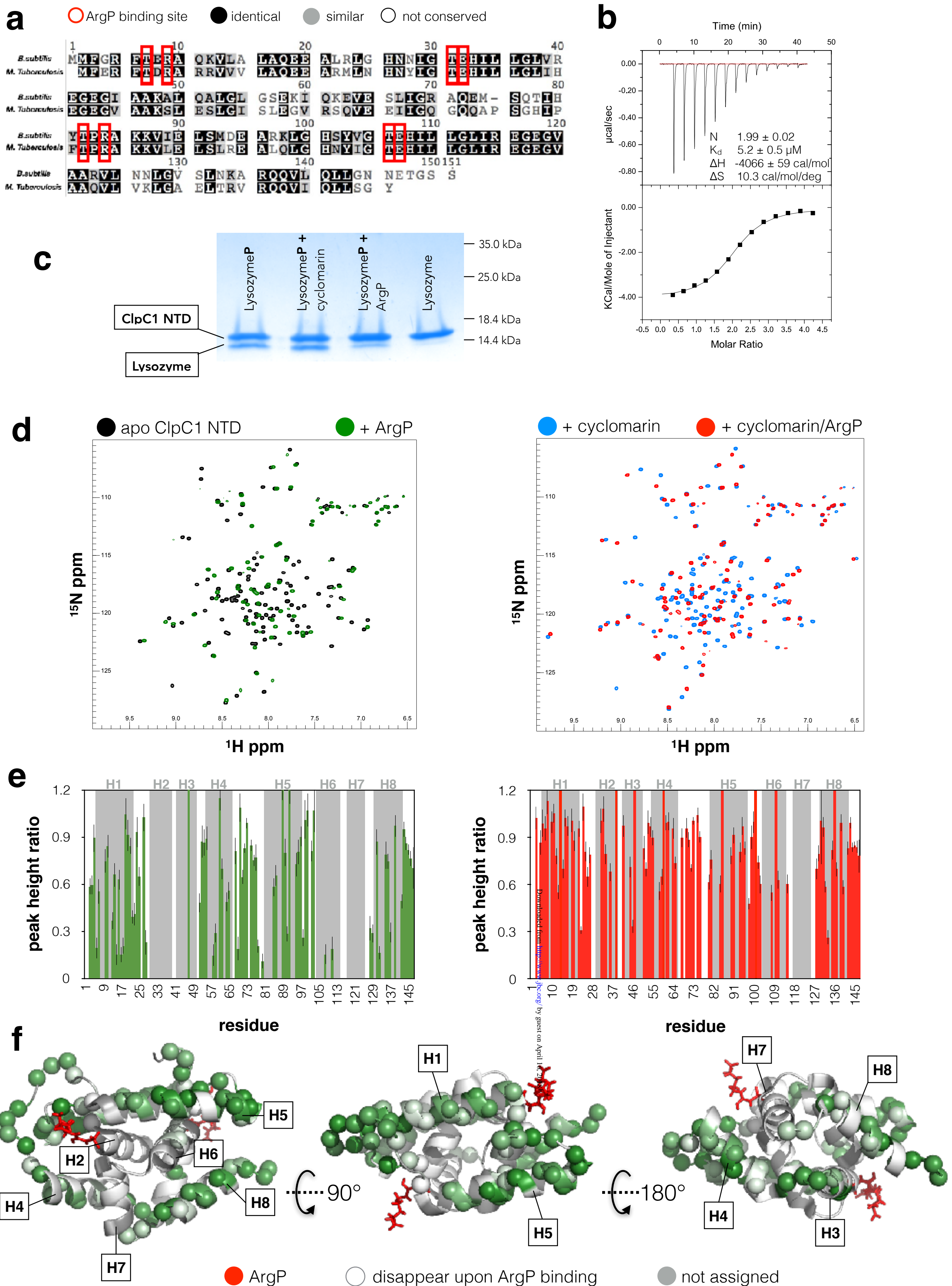


Figure 3

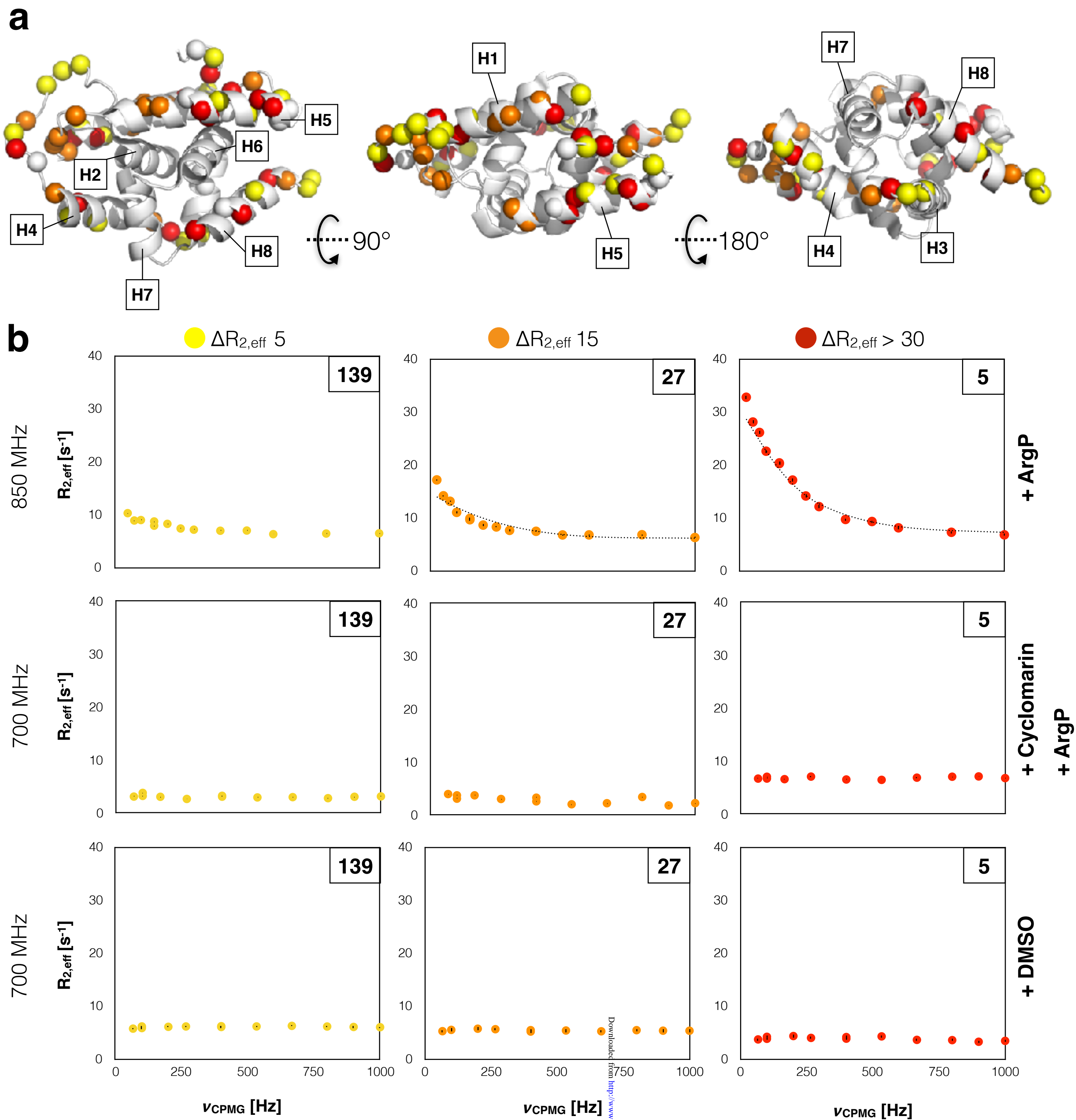


Figure 4

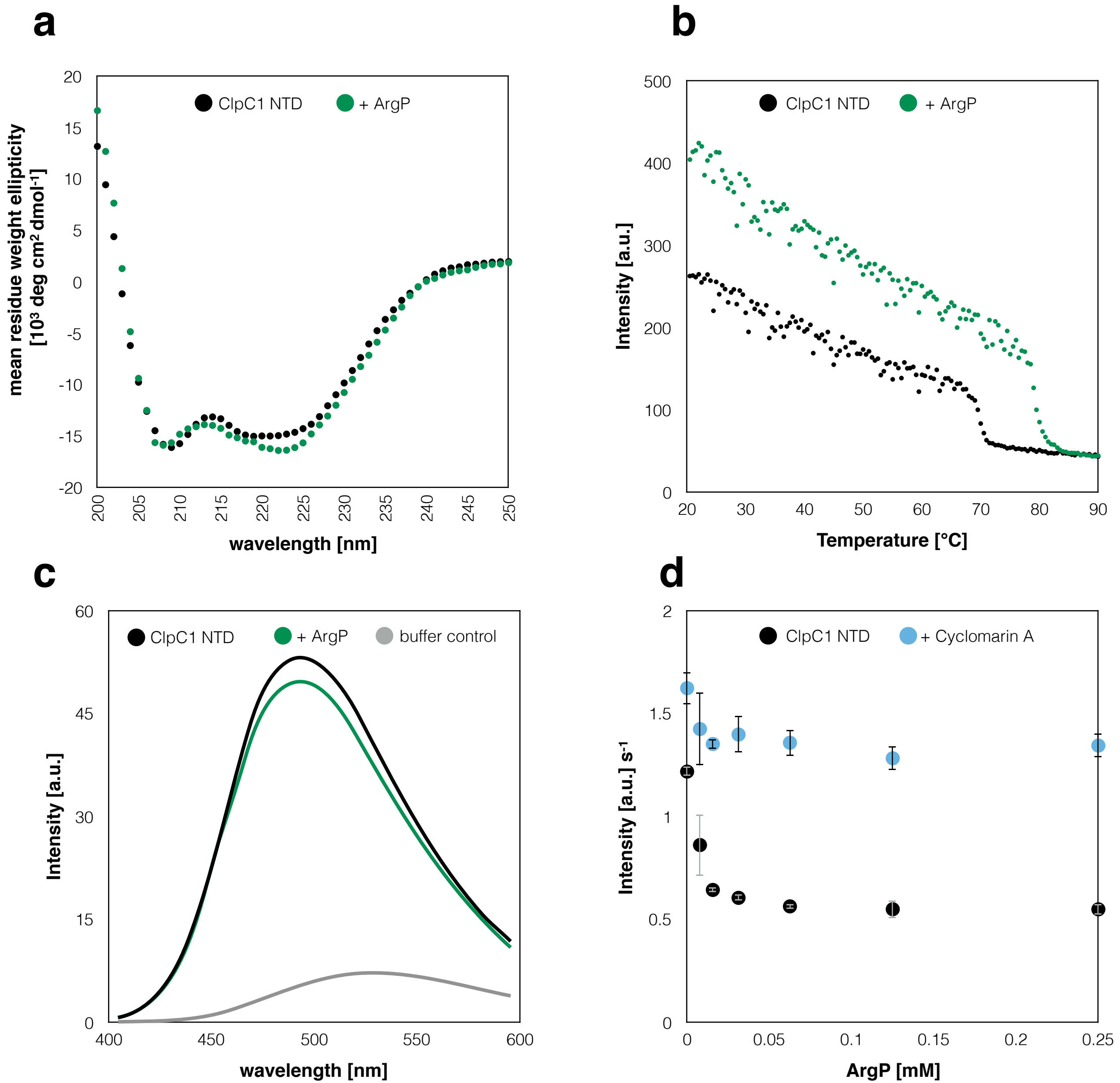


Figure 5

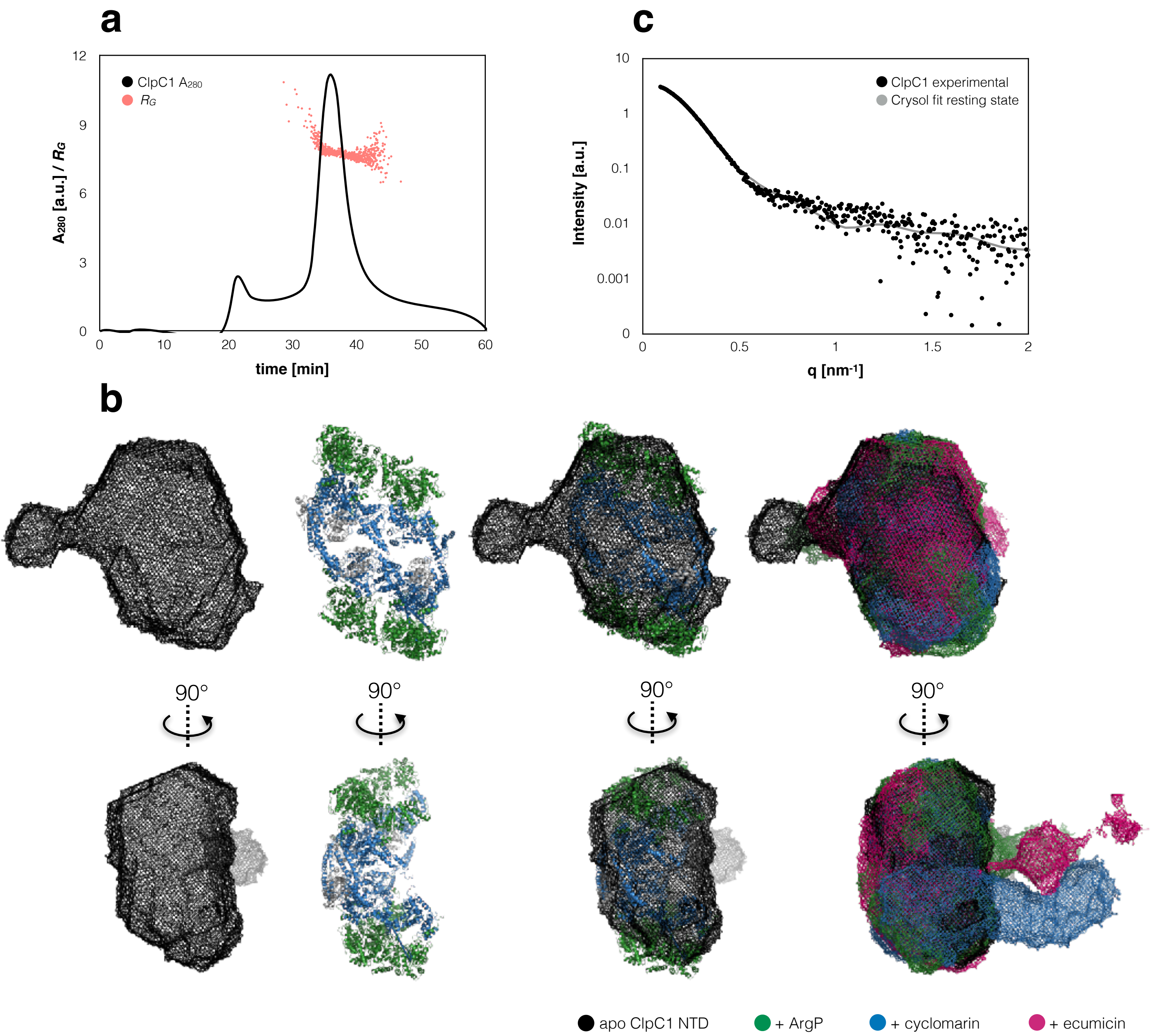


Figure 6

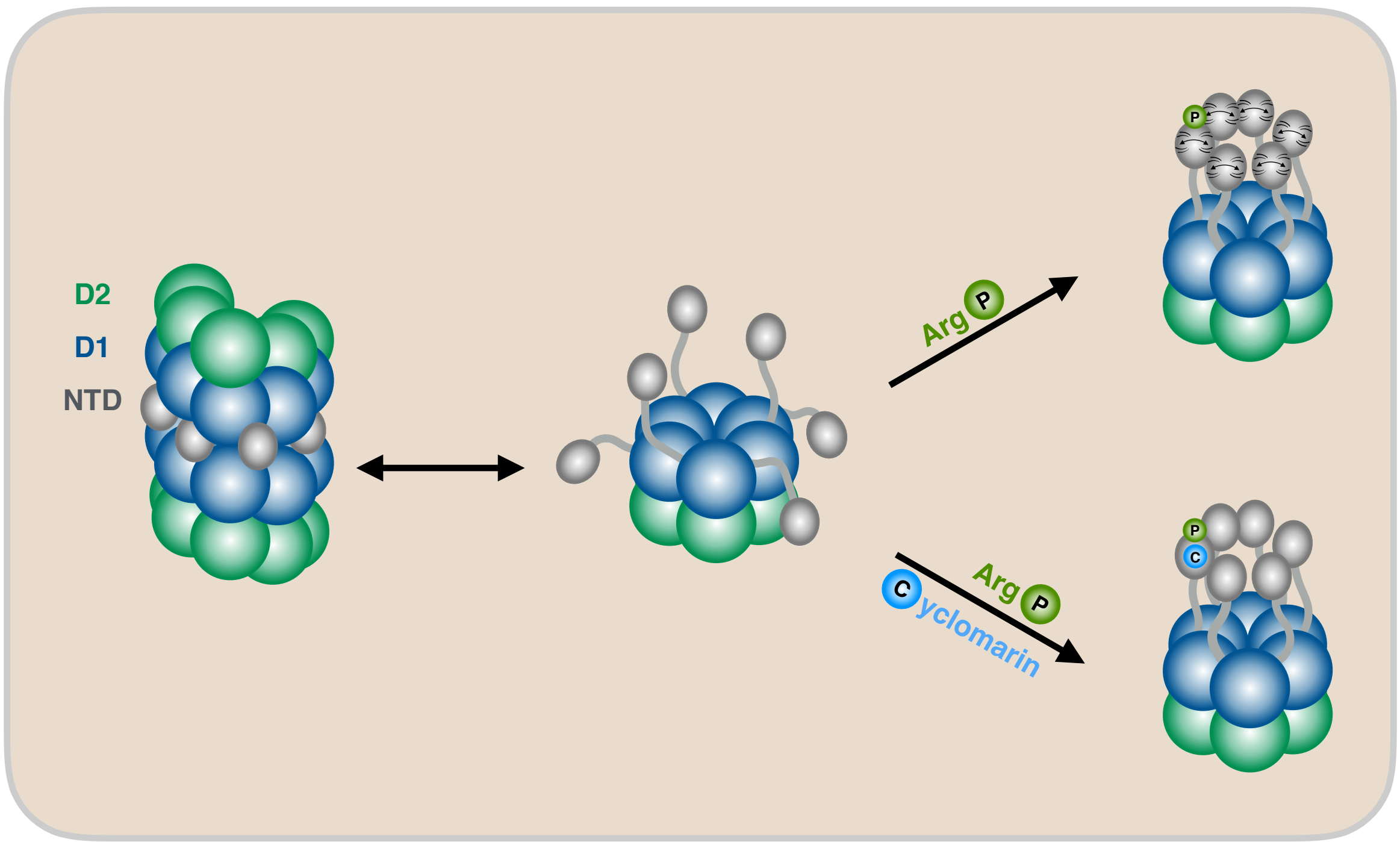


Figure 7

The antibiotic cyclomarin blocks arginine-phosphate–induced millisecond dynamics in the N-terminal domain of ClpC1 from *Mycobacterium tuberculosis*

Katharina Weinhäupl, Martha Brennich, Uli Kazmaier, Joel Lelievre, Lluís Ballell, Alfred Goldberg, Paul Schanda and Hugo Fraga

J. Biol. Chem. published online April 9, 2018

Access the most updated version of this article at doi: [10.1074/jbc.RA118.002251](https://doi.org/10.1074/jbc.RA118.002251)

Alerts:

- [When this article is cited](#)
- [When a correction for this article is posted](#)

[Click here](#) to choose from all of JBC's e-mail alerts